RSC Advances

PAPER

View Article Online
View Journal | View Issue

Cite this: *RSC Adv.*, 2017, **7**, 37349

Pitting resistivity of Ni-based bulk metallic glasses in chloride solution

Khadijah M. Emran * and Hanaa AL-Refai

Resistance of new $Ni_{70}Cr_{21}Si_{0.5}B_{0.5}P_8C_{\leq 0.1}Co_{\leq 1}Fe_{\leq 1}$ (VZ1) and $Ni_{72.65}Cr_{7.3}Si_{6.7}B_{2.15}C_{\leq 0.06}Fe_{8.2}Mo_3$ (VZ2) glassy alloys to pitting corrosion was studied in 0.25 M sodium nitrate solution, with or without addition of chloride ions, using electrochemical impedance spectroscopy (EIS), cyclic polarization (CP) and electrochemical frequency modulation (EFM) techniques. Pitting and passivation potentials, corrosion current density and corrosion rate were analyzed relative to the chloride ion concentration. Focusing on the anodic part of the CP scan, the Ni-based glassy alloys in neutral solution acquired passive behavior before the onset of rapid alloy dissolution at the pitting potential. This potential was greatly reduced by the addition of Cl^- ions. The aggressive ions led to a sharp increase of current at potentials significantly below the value required for pitting in the neutral medium and enhanced the formation and growth of the pits. A wider potential range free from pitting corrosion was observed for the VZ1 alloy. X-ray photoelectron spectroscopy (XPS), scanning electron microscopy (SEM), and atomic force microscopy (AFM) were conducted to assess the composition and morphology of the corrosion products and to provide supporting evidence for the electrochemical measurements.

Received 20th May 2017
Accepted 15th July 2017

DOI: 10.1039/c7ra05709a

rsc.li/rsc-advances

1 Introduction

Bulk metallic glasses (BMGs) are considered to be the materials of the future because of their disordered atomic structure and the absence of grain boundaries.[1,2] Ni-based glassy alloys are considered as one of the most important BMGs, having unique and unconventional characteristics.[3] The Ni-based glassy alloy has a good corrosion resistance in natural fresh water, excellent resistance to corrosion in alkaline media, such as sodium and potassium hydroxide, and has been used in various fields.[4] Ni–Cr-metalloid bulk glassy alloys, which exhibit superior corrosion resistance, have been studied in different aqueous media, including boiling 6N HNO_3 with or without Cr^{6+} ions.[5] They have also been intensively studied to further improve their corrosion resistance. For example, the formation of passive films on $Ni_{82.3}Cr_7Fe_3Si_{4.5}B_{3.2}$ and $Ni_{75.5}Cr_{13}Fe_{4.2}Si_{4.5}B_{2.8}$ in aqueous HCl and H_3PO_4 have been reported.[6,7]

Ni–Cr-metalloid bulk glassy alloys, which exhibit superior corrosion resistance, have been studied in different aqueous media, including boiling 6N HNO_3 with or without Cr^{6+} ions.[5] They have also been intensively studied to further improve their corrosion resistance. For example, the formation of passive films on $Ni_{82.3}Cr_7Fe_3Si_{4.5}B_{3.2}$ and $Ni_{75.5}Cr_{13}Fe_{4.2}Si_{4.5}B_{2.8}$ in aqueous HCl and H_3PO_4 have been reported.[6,7]

It is generally acknowledged that pitting is the most common and most hazardous form of corrosion. It is very dangerous, widespread, and difficult to detect.[8] The Cl^- ion is more aggressive than other halide ions because of its smaller diameter. It is readily adsorbed on weak areas of the passive film, resulting in the initiation of pitting.[9] Many studies of passivation and pitting corrosion resistance have been reported for Ni–Cr alloys in NaCl solution.[10–14] These studies have shown that the presence of an inner barrier layer (Cr_2O_3) is a primary factor for enforcing passivity and that a higher Cr content in the alloy enhances resistance to pitting corrosion.

The primary goal of this study was to characterize the susceptibility/resistance of the new VZ1 and VZ2 alloys to pitting corrosion processes. The study combined electrochemical frequency modulation (EFM), electrochemical impedance spectroscopy (EIS) and cyclic polarization (CP) measurements with surface analytical measurements using X-ray photoelectron spectroscopy (XPS), scanning electron microscopy (SEM), and atomic force microscopy (AFM) techniques. Comparison of the results for the two alloys under identical conditions can yield additional information on the influence of Cr percentage in Ni-based glassy alloys (as an alloying element) on corrosion resistance.

2 Experimental

Two new Ni-based BMG alloys with nominal compositions (wt%) of $Ni_{70}Cr_{21}Si_{0.5}B_{0.5}P_8C_{\leq 0.1}Co_{\leq 1}Fe_{\leq 1}$ (VZ1) and $Ni_{72.65}Cr_{7.3}Si_{6.7}B_{2.15}C_{\leq 0.06}Fe_{8.2}Mo_3$ (VZ2) were investigated in this work. These glassy alloys were produced by rapid solidification as ribbons of about 40–74.5 mm width and 25 μm thickness.

Chemistry Department, College of Science, Taibah University, Al-Madinah Al-Monawarah, Saudi Arabia. E-mail: kabdalsamad@taibahu.edu.sa

The test electrolytes used in the study were 0.25 M $NaNO_3$ solutions containing different concentrations (0.001, 0.01, 0.1, and 0.15 M) of NaCl, which were prepared from reagent grade chemical and double distilled water. All chemicals were obtained from Aldrich chemical company. The electrochemical measurements were performed in typical three-compartment glass cells containing three electrodes: the working electrode (WE), which was the alloy under study with a working area of 100 mm^2; the counter-electrode (CE) was a platinum wire; the reference electrode (RE) was saturated Ag/AgCl. Electrochemical measurements were conducted on an Interface 1000™, Gamry Potentiostat/Galvanostat/ZRA analyzer. The potential of the examined alloy was recorded as a function of time over a period of 1 h until it had become stable. For EFM analysis the baseline frequency was 0.1 Hz, input frequencies of 2 and 5 Hz were used with amplitudes of 10 mV over 4 cycles, bandwidth was $0.1 < \Delta f$ (Hz) < 1.5 and the corrosion process under investigation was passive. The EIS measurements were performed over the range of 800 kHz (initial frequency) to 0.1 Hz (final frequency), 10 points per decade. A small, alternating current (*e.g.*, 10 mV amplitude) was applied during the measurement to stimulate the current response from the alloy without affecting its performance. Cyclic polarization curves were obtained with a potential sweep rate of 1 mV s^{-1}. The potential was swept from cathodic to anodic directions after the impedance run from −800 mV to 1200 mV.

X-ray photoelectron spectroscopy (XPS) measurements were carried out using a monochromatic Al Kα X-ray source operating at 300 W (Kratos Axis Ultra DLD). The area of the analyzed surface was approximately 5 mm × 5 mm. Before analyses, the surfaces were cleaned by Ar^+ sputtering and the survey spectra were collected at a fixed analyzer pass energy of 160 eV.

The surface condition and chemical composition of the alloys surface after cyclic polarization were examined using a JEOL JSM-6000 scanning electron microscope (SEM). AFM measurements were carried out in contact mode with a constant scanning forces adjusted to 225 nN (10^{-9} N), a scanned area of 5 × 5 μm and resolution of 256 × 256 pixels.

3 Results and discussion

3.1 Impedance measurements after chloride addition

To investigate the impact of chloride ion on passive film thickness and susceptibility of VZ1 and VZ2 alloys to pitting corrosion in neutral solution in the passive potential range, different quantities concentrations (0.001, 0.01, 0.1, and 0.15 M) of NaCl were added to 0.25 M $NaNO_3$ solution at 27 °C after exposure duration of 1 h in test solution. The impedance plots for VZ1 and VZ2 alloys are shown in Fig. 1. As can be observed in Fig. 1a and b, similar complex impedance plots were obtained for VZ1 and VZ2 alloys at different concentrations, except for VZ1 in 0.25 M $NaNO_3$ alone, which was characterized by a straight capacitive upwards line that turned left towards negative values. This extended from intermediate frequencies down to the low frequency range corresponding to the passivation process.[15] There was only one slight deviation from a straight capacitive line at the high frequency range, indicating a fast charge transfer process at the metal/solution interfaces. The capacitive arc at low frequencies resulted from the diffusion through the porous surface film, which is a characteristic

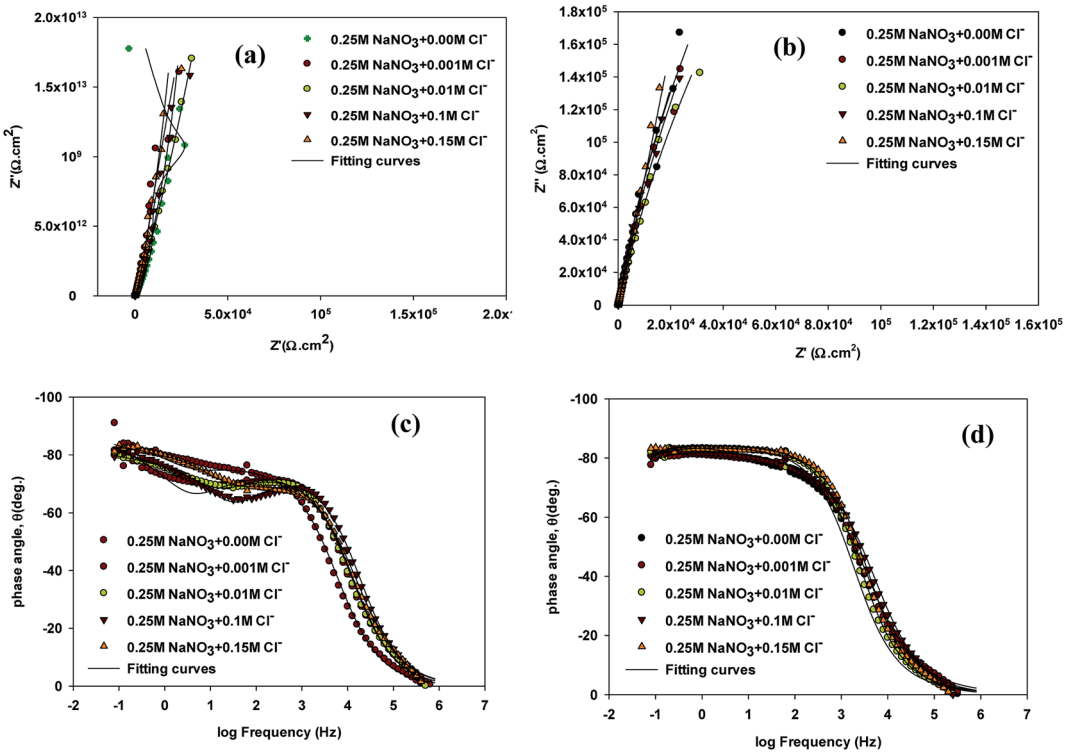

Fig. 1 Impedance plots of VZ1 and VZ2 alloys in different concentrations of NaCl at 27 °C.

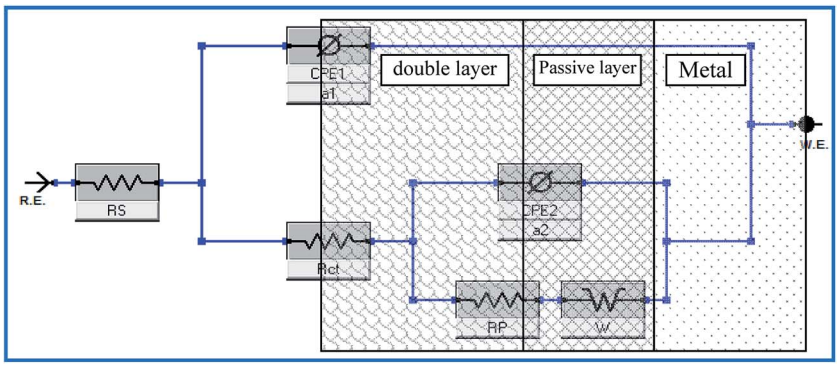

Fig. 2 Electrical equivalent circuit used to analyze the present experimental EIS data.

property of a passive surface. Moving towards the high frequency region, another small capacitive loop was observed, corresponding to a fast charge transfer process. The impedance plots for VZ2 alloy (Fig. 1a) were not substantially different from those of VZ1 alloy (Fig. 1b), but the passive film resistance of the VZ1 alloy was higher than that of the VZ2 alloy. This indicated that the different proportions of alloying elements (7.3% Cr and 8.2% Fe) decreased the impedance but did not change other aspects of the passivation behavior.

Bode plots exhibited two time constants, as shown in Fig. 1c and d. The capacitive loop in the high frequency region represents the electric charge transfer process. The second capacitive loop in the low frequency region is associated with a diffusion processes through the corrosion products and inside the pits.[16]

To interpret electrochemical behavior, the electrical circuit shown in Fig. 2 was used with a smallest error of fit of about χ^2 (10^{-3}) and a circuit description code (CDC) of $R_s(Q_1[R_{ct}(Q_2(R_f W))])$. The circuit model consisted of a parallel combination of a capacitor, $Q_1(CPE_1)$, and a charge transfer resistor, R_{ct}, in series with a resistor, R_s, representing the solution resistance. Another combination ($Q_2(R_fW)$) of a passive film capacitor, $Q_2(CPE_2)$, passive film resistance, R_f, and a Warburg impedance, W, representing the diffusion process, was included. The relevance of the use of diffusion/migration impedance to describe the passive film system has been demonstrated.[17] Fitted experimental data are plotted as solid lines in Fig. 1, and the values of the fitting parameters are presented in Table 1. The general trend for both two alloys for the variation of the values of the charge transfer resistance (R_{ct}), which is inversely proportional to the constant phase elements (CPE_1) of the double layer, with NaCl molar concentration was to decrease over the whole concentration range (0.001–0.15 M), Table 1. There was no indication of a critical concentration, suggesting that the chloride ion caused pitting corrosion. The polarization resistance of the inner barrier layer R_f was in the kΩ cm^2 range for VZ1 alloy in all media investigated, with a maximum value of 5.75 kΩ cm^2 at 0.001 M NaCl and a minimum value of 2.96 kΩ cm^2 at 0.15 M NaCl.

The R_{ct} values for the VZ2 alloy were lower than those measured for the VZ1 alloy because the passive layer could not cover the whole VZ2 alloy surface when the specimen was exposed in neutral solutions. The corrosion rate of the surface covered by the passive layer was lower than that of the surface without the passive layer (localized corrosion).[18] This clearly indicates that the morphology of the surface film microstructure is the crucial factor affording VZ1 alloy better intrinsic resistance to corrosion in chloride solutions. The R_{ct} values for both alloys in 0.25 M $NaNO_3$ containing different concentrations of Cl^- were several orders of magnitude lower, Table 1, than the values obtained for chloride-free solution, implying high corrosion behavior due to the severely corrosive nature of the Cl^- ion.

Table 1 Equivalent circuit parameters for the spontaneously formed passive film on VZ1 and VZ2 alloys as a function of NaCl concentrations at 27 °C

Alloys	Con. NaCl, M	R_{ct}, Ω cm^2	CPE_1, $Q_1 \times 10^{-5}$, Ω^{-1} cm^{-2} s^{n_1}	n_1	R_f, Ω cm^2	CPE_2, $Q_2 \times 10^{-5}$, Ω^{-1} cm^{-2} s^{n_2}	n_2
VZ1	**0.0**	3.40×10^8	1.03	0.88	2.42×10^5	2.31	0.90
	0.001	8.84×10^7	1.37	0.83	5.76×10^3	3.54	0.82
	0.01	9.94×10^6	1.23	0.84	3.05×10^3	3.59	0.86
	0.1	9.87×10^6	1.25	0.83	3.98×10^3	3.63	0.82
	0.15	8.70×10^6	1.29	0.81	2.96×10^3	4.37	0.78
VZ2	**0.0**	1.67×10^8	1.36	0.93	3.86×10^5	1.01	0.69
	0.001	7.06×10^7	1.10	0.93	5.01×10^3	2.91	0.90
	0.01	1.37×10^7	1.19	0.89	3.08×10^3	8.96	0.98
	0.1	3.74×10^6	1.50	0.89	5.26×10^3	7.96	0.90
	0.15	4.49×10^5	1.66	0.88	4.99×10^3	0.89	0.90

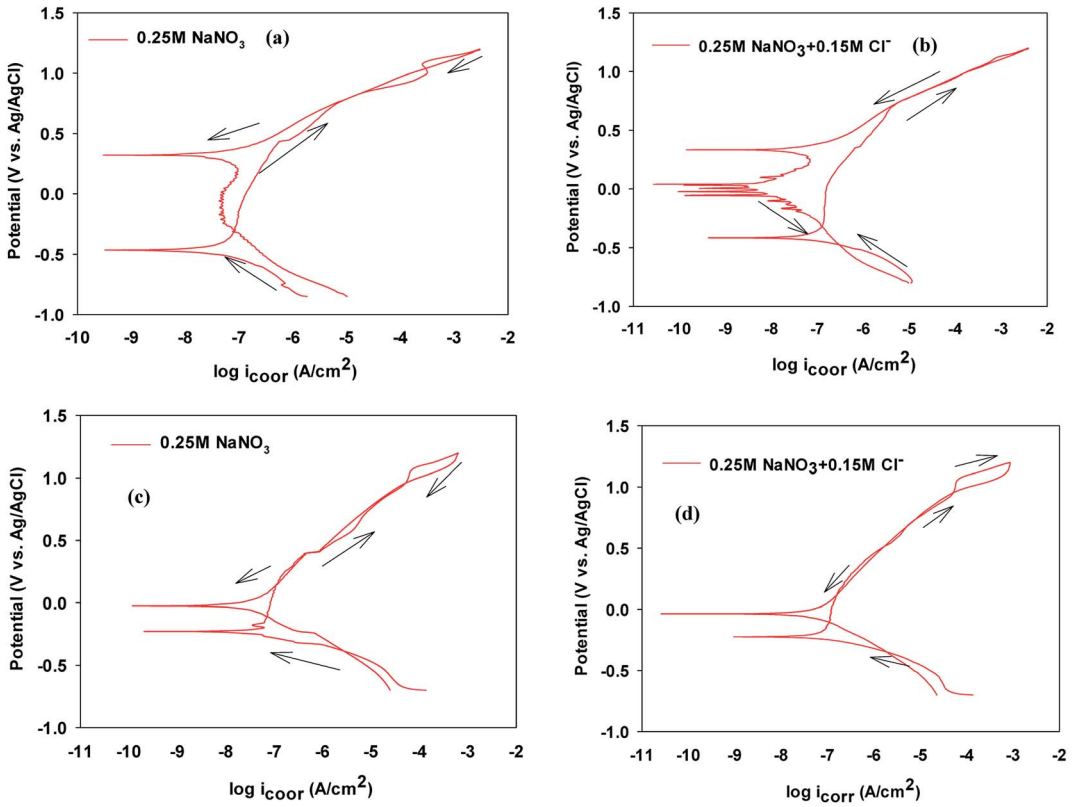

Fig. 3 Cyclic polarization curves of VZ1 and VZ2 alloys in the absence and presence of NaCl at 27 °C.

3.2 Cyclic polarization (CP) measurements after chloride addition

The cyclic polarization data recorded after immersing the VZ1 and VZ2 alloys for 1 h in 0.25 M $NaNO_3$ or for 1 h in 0.25 M $NaNO_3$ + 0.15 M NaCl are presented in Fig. 3a and b and in Fig. 3c and d, respectively. Table 2 shows an irregular shift of the corrosion potential (E_{corr}) for VZ1 toward more positive values, associated with increased corrosion current density, at higher Cl^- ion concentration. Comparatively, the corresponding values for the VZ2 alloy were almost unchanged (≤2 mV *vs.* Ag/AgCl). In addition, values of i_{corr} for VZ1 increased as the Cl^- concentration increased, but were still lower than the i_{corr} values for the VZ2 alloy because the higher Cr content (21%) confers resistance to the corrosive action of Cl^- ions. Consequently, the dissolution process is slow. Focusing on the anodic part of the cyclic polarization scan, passive behavior was observed for all samples before the onset of rapid alloy dissolution at break down potential (pitting potential, E_{pit}). At E_{pit}, the current rises sharply and stable pits begin to grow. Between E_{pit} and the repassivation or protection potential (E_{rep}), no new pits develop. Initiation and propagation of pits continued until

Table 2 The corrosion kinetic parameters obtained from CP and EFM techniques for VZ1 and VZ2 alloys as a function of NaCl at 27 °C

		EFM					CP				
Alloys	Con. NaCl, M	i_{corr}, μA cm^{-2}	$-\beta_c$, mV per decade	Corrosion rate × 10^{-3}, mmpy	CF-2	CF-3	$-E_{corr}$, mV	i_{corr}, μA cm^{-2}	$-\beta_c$, mV per decade	E_{pit}, mV	E_{rep}, mV
VZ1	**0.0**	0.08	120	1.40	1.40	2.64	465	0.02	110	447	1045
	0.001	0.14	110	2.11	1.19	2.37	453	0.02	111	192	1051
	0.01	0.19	119	26.6	1.57	2.02	400	0.04	112	160	1020
	0.1	0.43	122	30.2	1.46	2.16	440	0.04	116	131	1001
	0.15	0.49	120	32.3	1.23	2.47	415	0.09	114	131	1043
VZ2	**0.0**	0.09	59	1.50	1.89	2.98	231	0.03	80	231	980
	0.001	0.15	56	2.57	1.19	2.37	225	0.04	71	187	1010
	0.01	0.35	56	36.4	1.67	2.34	223	0.04	75	143	1010
	0.1	0.35	65	39.2	1.46	2.46	222	0.05	72	41	980
	0.15	0.68	63	39.6	1.78	2.47	220	0.07	76	34	966

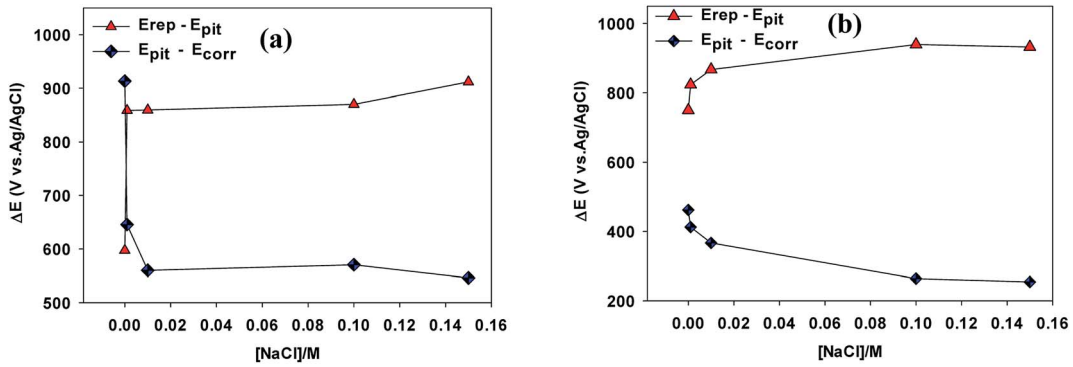

Fig. 4 Variation of the different ranges defined between E_{corr}, E_{pit} and E_{rep} as a function of Cl^- ion concentrations for VZ1 and VZ2 alloys at 27 °C.

the reverse potential scan reached the repassivation potential, E_{rep}, at which point the pits were repassivated. Below E_{rep} pits do not continue to grow.[19,20] These pits will not initiate at E_{corr} because the repassivation potential (E_{rep}) is more noble than the corrosion potential.

The potential difference ($E_{pit} - E_{rep}$) can be used as an approximate measure of the hysteresis loop area, where smaller potential differences represent better resistance of the alloy to pitting corrosion.[21] Higher values of the potential difference ($E_{pit} - E_{corr}$) exhibit a wider potential range free of pitting corrosion under these conditions.[22]

As can be seen in Fig. 4a, in the absence of NaCl the hysteresis loop area ($E_{pit} - E_{rep}$) value for VZ1 alloy was about 597.20 mV *vs.* Ag/AgCl, compared to a value of 750 mV *vs.* Ag/AgCl for VZ2 alloy in 0.25 M $NaNO_3$. These values increased gradually for both alloys when NaCl was added to the neutral solutions, reflecting the better pitting corrosion resistance of VZ1 alloy. In addition, the potential range free of pitting corrosion for the VZ1 alloy curve ($E_{pit} - E_{corr}$) was wider than that of the VZ2 alloy. The values were 913.30 mV *vs.* Ag/AgCl for VZ1 and 461.6 mV *vs.* Ag/AgCl for VZ2 alloy in chloride-free solution. This confirms that the degree of corrosion was lower in VZ1 alloy compared to VZ2 alloy because the higher proportion of Cr (21%) increased resistance to pitting corrosion. The potential range decreased gradually as the Cl^- ion concentration increased. These results indicate that the susceptibility of the alloys to pitting corrosion at higher chloride ion concentrations is due to Cl^- ion aggravating the conditions for formation and growth of pits.[23] The Cl^- ion is more aggressive than other halide ions due to its smaller diameter and consequent ability to more readily penetrate the passive film.[9]

The linear relationships between E_{pit} values and Cl^- ion concentration on the cyclic polarization curves for VZ1 and VZ2 alloys are shown in Fig. 5a and b. It can be seen that E_{pit} shifted to more negative values (active direction) for both alloys and decreased logarithmically as the chloride ion concentration increased, according to eqn (1):[24]

$$E_{pit} = a + b \log C_{Cl^-} \quad (1)$$

where a and b are constants depending on the Ni-based glassy alloy/NaCl solution system and a represents a measure of the aggressiveness of the Cl^- ion.[9,23]

Passive film breakdown and pit initiation can be explained by an adsorption mechanism. During adsorption, pits initiate at weak sites of the passive film where Cl^- ions displace oxygen and form soluble metal–anion complexes. This enhances transfer into the electrolyte leading to local thinning of the passive film until complete film removal.[9] The alloy surface is exposed to the electrolyte and a galvanic cell is produced in which the base elements in the alloy act as the anode and the passive layer acts as the cathode.

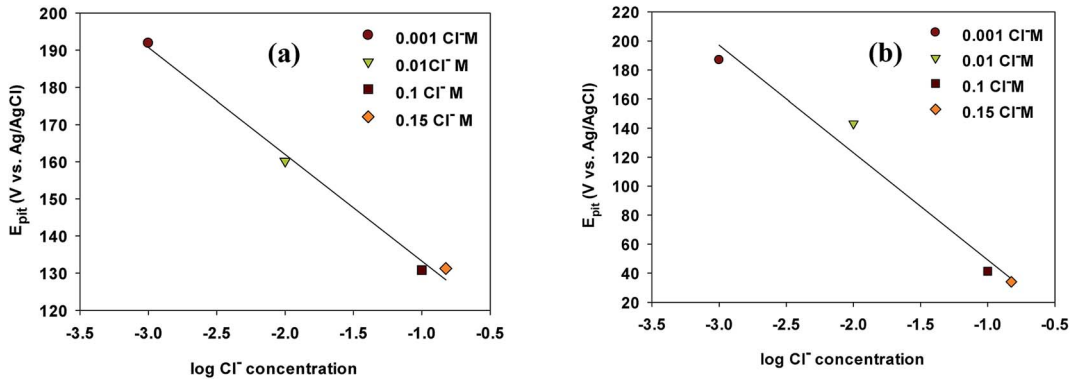

Fig. 5 Pitting potential of Ni-base glassy alloys in 0.25 M $NaNO_3$ at varying concentrations of NaCl for VZ1 and VZ2 alloys at 27 °C.

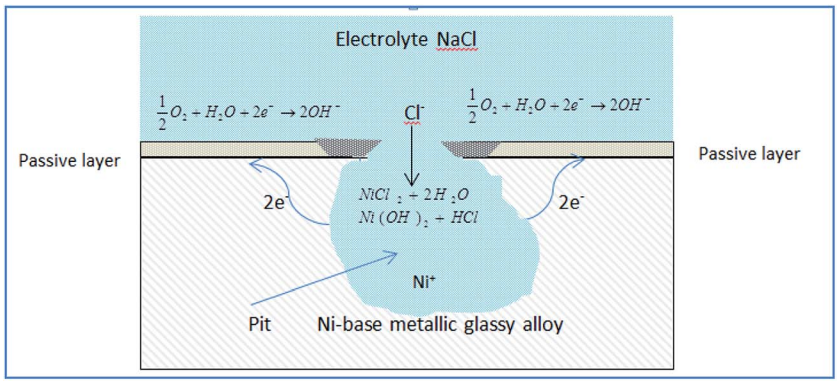

Fig. 6 Schematic of an actively growing pit in Ni-based metallic glassy alloy.

Fig. 6 shows a propagating pit (actively growing) in the Ni-based glassy alloy/NaCl solution system.

According to Fig. 6, anodic reactions within the pit are described by (eqn (2)):

$$Ni \rightarrow Ni^{+2} + 2e^- \quad (2)$$

The electrons flow to the cathode (passivated surface) where they are consumed in the cathodic reaction (eqn (3)):

$$\frac{1}{2}O_2 + H_2O + 2e^- \rightarrow 2OH^- \quad (3)$$

As a result of cathodic and anodic reactions, the electrolyte within the pit acquires positive charge while the electrolyte surrounding the pit becomes negatively charged. The positively charged pit attracts negative chloride ions and soluble metal–anion complexes are formed eqn (4):

$$NiCl_2 + 2H_2O \rightarrow Ni(OH)_2 + HCl \quad (4)$$

The reaction between Ni^{2+} and water increases the acidity of the electrolyte inside the pit, accelerating the corrosion process, and the corrosion products that form around the pit separate its electrolyte.[23]

3.3 Electrochemical frequency modulation (EFM) measurements

Based on the data presented in Table 2, the VZ1 alloy exhibited outstanding corrosion resistance, having low corrosion rate values (<0.02 mmpy (ref. 25)) at Cl^- ion concentrations of 0.001 and 0.01 M. At Cl^- ion concentrations of 0.1 and 0.15 M, it exhibited excellent corrosion resistance (0.02–0.1 mmpy (ref. 25)). The VZ2 alloy at 0.001 M Cl^- ion concentration exhibited outstanding corrosion resistance (<0.02 mmpy (ref. 25)), whereas it exhibited excellent corrosion resistance (0.02–0.1 mmpy (ref. 25)) at NaCl concentrations ranging from 0.001 to 0.15 M.

It should be noted that the calculated values of i_{corr} obtained by EFM were higher than the values obtained from the polarization measurements. It is quite easy for the perturbation frequency in this Ni-based glassy alloy/NaCl solution system to be too high, which will cause excessive capacitive behavior of the electrochemical double layer on the current response and result in polarization resistance that is too low and a corrosion rate that is too high.[26] To avoid the capacitive influence, the frequency should be as low as possible. The causality factors were determined and found to be very close to the theoretical

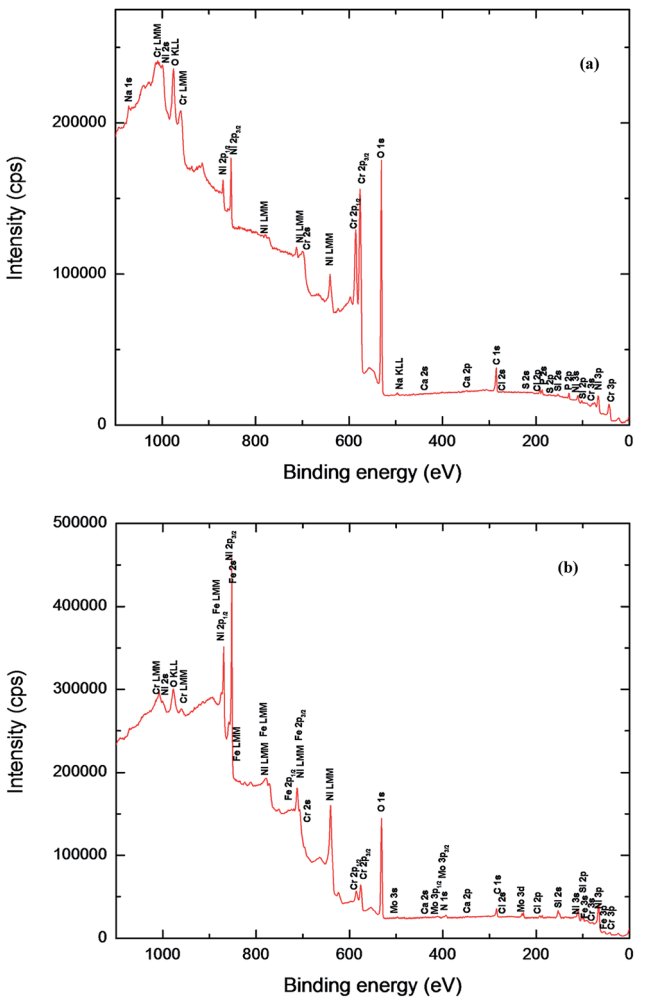

Fig. 7 XPS survey spectra of Ni-based glassy alloys in 0.25 M $NaNO_3$ solution at 27 °C; (a) VZ1 alloy, (b) VZ2 alloy.

values according to EFM theory. Sometimes, deviation in causality factor values can be due to high resistivity of the studied alloy. The three different electrochemical techniques showed similar behavior.

3.4 Morphological and structural characterizations

3.4.1 X-ray photoelectron spectroscopy (XPS) analysis of Ni-based alloys. The XPS survey spectra of passive films in 0.25 M $NaNO_3$ solution at 27 °C showed the presence of mainly nickel, chromium, iron, and oxygen signals (Fig. 7). Analysis of the Ni $2p_{3/2}$ spectra after treatment, Fig. 8a, showed peaks corresponding to the binding energy of metallic Ni at 852.3 eV. Peaks in the Ni $2p_{3/2}$ spectra corresponding to divalent nickel (Ni^{2+}) at 853.3 eV after treatment in neutral solution indicated that NiO was involved in the formation of passive film on the Ni-based glassy alloys. After the treatment, the Cr $2p_{3/2}$ spectra (Fig. 8b) contained peaks at 576.3 eV (trivalent chromium, Cr^{3+}) corresponding to the binding energy (BE) of chromium oxide (Cr_2O_3), which is in agreement with values obtained by other researchers.[10,27] Additionally, peaks in the range of 576.3–579.7 eV could be attributed to various chromium oxides in the hydrated chromium oxyhydroxide film [$CrO_x(OH)_{3-2x}\cdot nH_2O$] according to literature data.[28,29] These compounds would improve the corrosion resistance of the Ni-based glassy alloys.

The strong BE peaks found at 711.6 eV in the Fe $2p_{3/2}$ spectra (Fig. 8c) can be assigned to trivalent iron compounds such as Fe_2O_3 and/or FeOOH.[30] The analysis of the O 1s spectra (Fig. 8d) can be separated into four distinct components. The peak at about 529.9 eV corresponds to the binding energy of NiO and the peak at 530.3 eV may be due to the oxygen atom bonded to Cr^{3+} in the various chromium oxides.[10] The peak at 531.3 eV is due to O^{2-}, which confirms the presence of an oxygen atom bonded to Fe^{3+} in Fe_2O_3. The peak observed at 532.7 eV is attributed to an OH^- group bonded to Fe^{3+} in FeOOH.[30] Passive films on the VZ1 alloy may be different in structure and composition compared to the passive films formed on VZ2 alloy. The passive films on Ni–Cr alloys are reported to be composed of Cr_2O_3 and NiO. Jabs *et al.*[31] reported that the passive films formed on Ni–(20, 34)Cr alloys in 1 M NaOH solution had a duplex layered structure composed of inner Cr_2O_3 and outer NiO layers. Boudin *et al.*[32] also proposed a duplex layered structure with inner Cr_2O_3 and outer $Ni(OH)_2$ or Ni oxyhydroxide layers for the passive films formed on Ni–(5.6–27.3)Cr alloys in pH 9.2 borate solution. As mentioned above and according to XPS analyses of Ni–Cr alloys,[11,13,33] passive films formed on VZ1 alloy are commonly described by a duplex layer of Cr_2O_3/NiO, while passive films on VZ2 alloy are considered to be composed of NiO, Cr_2O_3, Fe_2O_3, and FeOOH.

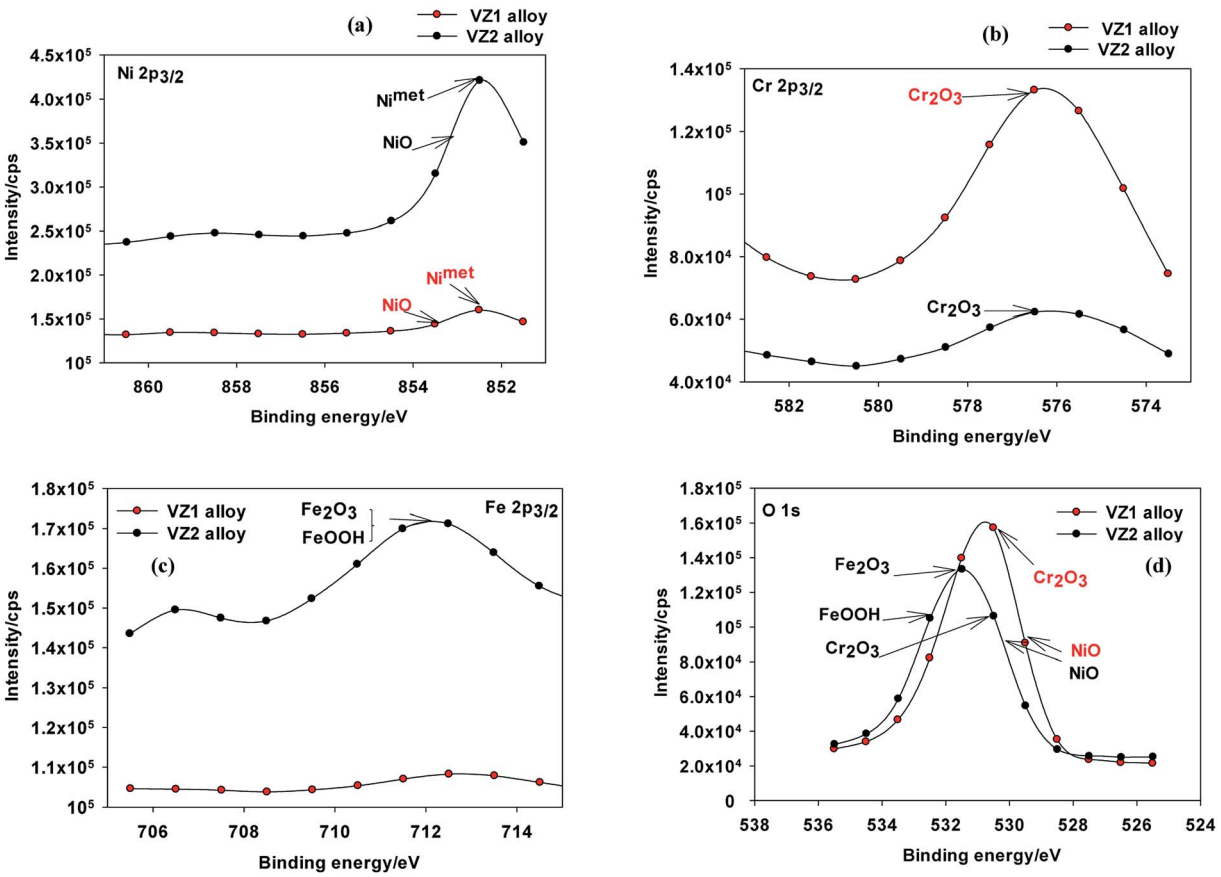

Fig. 8 XPS spectra of passive films formed on Ni-based glassy alloys in 0.25 M $NaNO_3$ solution at 27 °C; (a) Ni $2p_{3/2}$, (b) Cr $2p_{3/2}$, (c) Fe $2p_{3/2}$, and (d) O 1s.

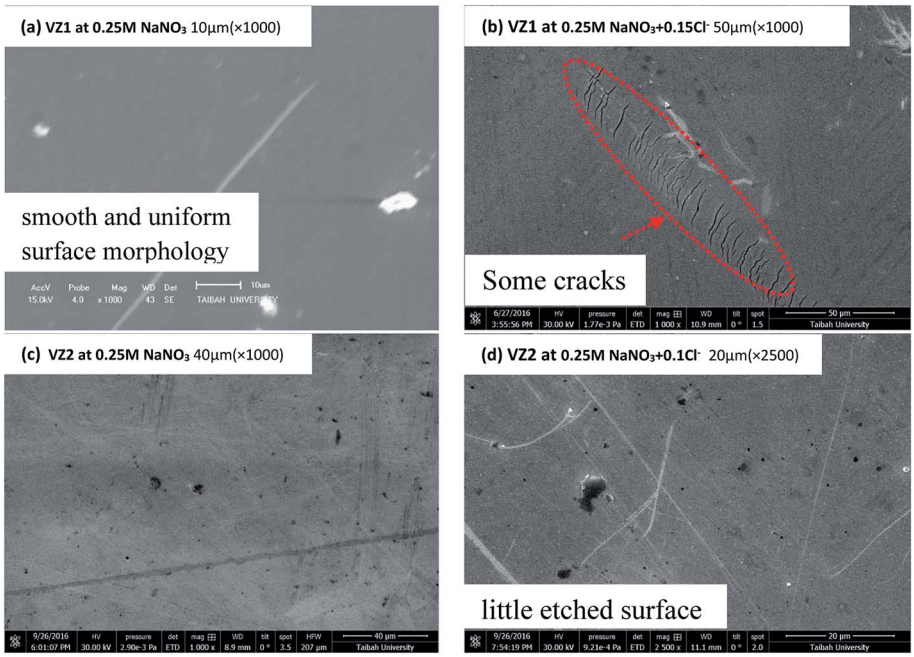

Fig. 9 SEM morphology of Ni-based glassy alloys before and after chloride ion addition at 27 °C.

3.4.2 Scanning electron microscopy (SEM) analyses of Ni-based alloys. The SEM images after cyclic polarization experiments on passive films exposed for 1 h in 0.25 M $NaNO_3$ and for 1 h in 0.25 M $NaNO_3$ + 0.15 M NaCl are shown in Fig. 9. VZ1 alloy in 0.25 M $NaNO_3$ is the only material presenting a smooth and uniform surface morphology rather than pit formation as observed on VZ2 alloy (Fig. 9a and c). This is indicative of the high corrosion resistance and passivating nature of the VZ1

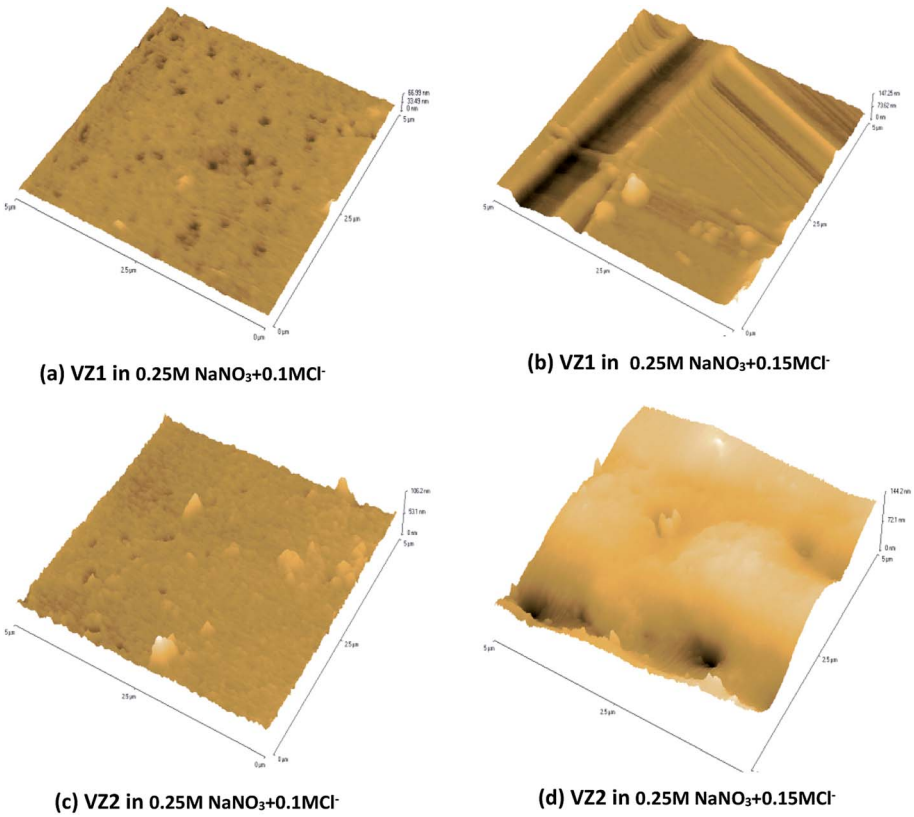

Fig. 10 AFM topography images of Ni-based glassy alloys in different concentrations of NaCl at 27 °C.

amorphous ribbon sample. Some cracks were observed on the passive layer formed on VZ1 alloy (Fig. 9b) at a high concentration of Cl^- ions (0.15 M NaCl + 0.25 M $NaNO_3$). Comparing the microstructures in Fig. 9c and d, which correspond to VZ2 before and after chloride ion addition, it is clear that the chloride containing neutral solution has a slight effect: samples containing 0.15 M NaCl show the typical presentation of a slightly etched surface resulting from the corrosive attack of chloride ions.

3.4.3 Atomic force microscopy (AFM) topographic images of Ni-based alloys. No micro pits were observed on the passivated VZ1 specimen in the 3D image. The roughness average, R_a, values were 1.08 nm and 1.65 nm for VZ1 and VZ2 alloys, respectively. After immersion in the Cl^- ion solutions, small pits were present in the passive layers and the depth of the pits increased as the Cl^- ion concentration was increased (Fig. 10). The surface roughness of the VZ1 alloy increased from 1.64 nm to 11.48 nm as the Cl^- ion concentration in neutral solution was increased from 0.001 M to 0.15 M. In comparison, the surface roughness of VZ2 alloy increased from 3.09 nm to 8.79 nm. A significant increase was observed in the overall spatial roughness of Ni-based glassy alloys treated with NaCl solutions compared to untreated alloys (in 0.25 M $NaNO_3$). This is attributed to the difference in micro-structural roughness. As the NaCl concentration is increased, it is more likely that pitting corrosion is accelerated and the surface of the alloy acquires a 'hills and valleys' topology.

4. Conclusion

Two Ni-based bulk metallic glasses, with nominal compositions of $Ni_{70}Cr_{21}Si_{0.5}B_{0.5}P_8C_{\leq 0.1}Co_{\leq 1}Fe_{\leq 1}$ (VZ1) and $Ni_{72.65}Cr_{7.3}Si_{6.7}B_{2.15}C_{\leq 0.06}Fe_{8.2}Mo_3$ (VZ2), were studied in aqueous 0.25 M sodium nitrate solution with and without addition of chloride ion. EIS analysis revealed that the VZ1 alloy exhibited higher corrosion resistance compared to the VZ2 alloy. This was attributed to the formation of passive films with a duplex structure composed of an outer porous layer at high frequency and an inner compact barrier layer of Cr_2O_3 at lower frequency. Enhanced corrosion of Ni-based glassy alloys occurred at higher Cl^- ion concentrations, since the potential range of passivity was shortened and both the pitting (E_{pit}) and repassivation (E_{rep}) potentials became less noble. VZ1 alloy showed a relatively lower value of passive current density and a smaller anodic hysteresis loop area compared to VZ2 alloy in neutral chloride media. This was due to the higher Cr content (21%), which enhances Cr_2O_3 formation. Alloying elements are very important factors to stabilize an alloy against localized corrosion. The presence of Cr (21%) leads to increased corrosion resistance for nickel-based glassy alloys. It accumulates in the passive layer as Cr_2O_3 or oxyhydroxide.

Acknowledgements

The authors would like to thank Dr Hartmann Thomas from Vacuumschmelze GmbH for providing the specimens.

References

1 E. Axinte, *Mater. Des.*, 2012, **35**, 518–556.
2 J. P. Chu, J. Jang, J. Huang, H. Chou, Y. Yang, J. Ye, Y. Wang, J. Lee, F. Liu and P. Liaw, *Thin Solid Films*, 2012, **520**, 5097–5122.
3 Y. Zeng, C. Qin, N. Nishiyama and A. Inoue, *J. Alloys Compd.*, 2010, **489**, 80–83.
4 H. Kim, D. Mitton and R. Latanision, *Corros. Sci.*, 2010, **52**, 801–809.
5 C. Qin, K. Asami, H. Kimura, W. Zhang and A. Inoue, *Electrochim. Acta*, 2009, **54**, 1612–1617.
6 S. Arab and K. Emran, *Phys. Chem. News*, 2009, **50**, 130–138.
7 S. T. Arab, K. M. Emran and H. A. Al-Turaif, *J. Saudi Chem. Soc.*, 2014, **18**, 169–182.
8 J. Bhandari, F. Khan, R. Abbassi, V. Garaniya and R. Ojeda, *J. Loss Prev. Process Ind.*, 2015, **37**, 39–62.
9 J. Soltis, *Corros. Sci.*, 2015, **90**, 5–22.
10 J. Grosseau-Poussard, J. Dinhut, J. Silvain and R. Sabot, *Appl. Surf. Sci.*, 1999, **151**, 49–62.
11 A. C. Lloyd, J. J. Noël, S. McIntyre and D. W. Shoesmith, *Electrochim. Acta*, 2004, **49**, 3015–3027.
12 M. Rao, *Mater. Corros.*, 2009, **60**, 49–52.
13 P. Jakupi, D. Zagidulin, J. Noël and D. Shoesmith, *Electrochim. Acta*, 2011, **56**, 6251–6259.
14 B. Ter-Ovanessian, N. Mary and B. Normand, *J. Electrochem. Soc.*, 2016, **163**, C410–C419.
15 M. Slemnik, *Anti-Corros. Methods Mater.*, 2008, **55**, 20–26.
16 N. Mahato and M. Singh, *Port. Electrochim. Acta*, 2011, **29**, 233–251.
17 B. Ter-Ovanessian, C. Alemany-Dumont and B. Normand, *Electrochim. Acta*, 2014, **133**, 373–381.
18 H. Li, H. Yu, T. Zhou, B. Yin, S. Yin and Y. Zhang, *Mater. Des.*, 2015, **84**, 1–9.
19 W. Peter, R. Buchanan, C. Liu, P. Liaw, M. Morrison, J. Horton, C. Carmichael and J. Wright, *Intermetallics*, 2002, **10**, 1157–1162.
20 Y. Chen, L. Chou and H. Shih, *J. Mater. Sci. Eng. A*, 2005, **396**, 129–137.
21 H. Liu, Y. Leng, G. Wan and N. Huang, *Surf. Coat. Technol.*, 2011, **206**, 893–896.
22 E. Kikuti, R. Conrrado, N. Bocchi, S. R. Biaggio and R. C. Rocha-Filho, *J. Braz. Chem. Soc.*, 2004, **15**, 472–480.
23 R. T. Loto, *J. Mater. Environ. Sci.*, 2013, **4**, 448–459.
24 W. A. Badawy, K. M. Ismail and A. M. Fathi, *Electrochim. Acta*, 2005, **50**, 3603–3608.
25 M. G. Fontana, Corrosion engineering, Tata McGraw-Hill Education, 2005.
26 L. Han and S. Song, *Corros. Sci.*, 2008, **50**, 1551–1557.
27 S. Ningshen, M. Sakairi, K. Suzuki and S. Ukai, *Corros. Sci.*, 2014, **78**, 322–334.
28 B.-P. Zhang, H. Habazaki, A. Kawashima, K. Asami and K. Hashimoto, *Corros. Sci.*, 1992, **33**, 1519–1528.
29 S. T. Arab, K. M. Emran and H. A. Al-Turaif, *J. Korean Chem. Soc.*, 2012, **56**, 448–458.

30 P. Singh, V. Srivastava and M. Quraishi, *J. Mol. Liq.*, 2016, **216**, 164–173.
31 T. Jabs, P. Borthen and H. H. Strehblow, *J. Electrochem. Soc.*, 1997, **144**, 1231–1243.
32 S. Boudin, J. L. Vignes, G. Lorang, M. Da Cunha Belo, G. Blondiaux, S. Mikhailov, J. Jacobs and H. Brongersma, *Surf. Interface Anal.*, 1994, **22**, 462–466.
33 H. Jang and H. Kwon, *ECS Trans.*, 2007, **3**, 1–11.